Spontaneous charge-ordered state in Bernal-stacked bilayer graphene

Xiu-Cai Jiang, Ze-Yi Song, Ze Ruan, and Yu-Zhong Zhang *

Shanghai Key Laboratory of Special Artificial Microstructure Materials and Technology, School of Physics Science and Engineering, Tongji University, Shanghai 200092, People's Republic of China

(Received 17 July 2023; revised 29 December 2023; accepted 8 February 2024; published 7 March 2024)

We propose that a weakly spontaneous charge-ordered insulating state probably exists in Bernal-stacked bilayer graphene, which can account for experimentally observed nonmonotonic behavior of resistance as a function of the gated field, namely, the gap closes and reopens at a critical gated field. The underlying physics is demonstrated by a simple model on a corresponding lattice that contains the nearest intralayer and interlayer hoppings, electric field, and staggered potential between different sublattices. Combining density functional theory calculations with model analyses, we argue that the interlayer van der Waals interactions cooperating with ripples may be responsible for the staggered potential, which induces a charge-ordered insulating state in the absence of the electric field.

DOI: 10.1103/PhysRevResearch.6.013255

I. INTRODUCTION

Bilayer graphene has been extensively studied for more than a decade. While fascinating progresses such as discovery of the integer quantum Hall effect [1,2], superconductivity [3,4], higher-order topological insulators [5], tunable excitons [6,7], and topological valley transport [8], induced by external fields [9–14], doping [15,16], and twist [17–19] have been reported, the ground state of Bernal-stacked bilayer graphene (BBG) remains controversial. Originally, BBG was thought to be a semimetal with massive Dirac cones at the Fermi level. Additionally, a gated field applied perpendicular to the plane breaks the symmetry between the top and bottom layers of BBG, rendering it an insulator, which has been confirmed by transport [10,12] and photoemission experiments [20,21]. Then, the gap should increase monotonously as a function of the applied gated electric field [22–25]. However, this is challenged by intriguing experimental observations on ultraclean suspended BBG that resistance varies nonmonotonously with the gated electric field at low temperatures [14,26–28], suggesting the presence of an intrinsic gap that closes and then reopens when an electric field is applied.

So far, much effort has been made to understand the discrepancy. Starting with the intrinsic gap at zero field, various possible candidate states, which stem from different origins, have been proposed. Using methods such as quantum Monte Carlo, functional renormalization group, etc., a layered antiferromagnetic (LAF) state has been suggested as a candidate state in BBG, which is favored by on-site Coulomb interactions [29–33]. By calculating the properties of Landau level $n = 0$ with spin and valley degree of freedom, a canted antiferromagnetic (CAF) state is suggested to be stabilized by isospin anisotropy of electron-electron and electron-phonon interactions [34]. Besides, the quantum spin Hall (QSH) state [33,35] and quantum anomalous Hall (QAH) state [36] are also considered as two potential candidate states with gap opening at zero field, which are favored by spin-orbit coupling and zero-point fluctuations, respectively. Recently, taking short-range interactions into account, a candidate state with the coexistence of nematic and antiferromagnetic states has also been proposed [37].

However, despite numerous investigations, a definitive explanation for the phenomenon that resistance varies nonmonotonously with an electric field remains elusive, which is probably due to the following two reasons. On one hand, most of the previous studies focus on the ground state at zero field, where there are many competing candidate states with very close energies [31]. Consequently, the ground state strongly relies on delicate details of the microscopic model [33,37–41] that a specific perturbation may favor a particular candidate state as introduced above. Although these studies suggest the presence of a magnetic ground state at zero field [42], there is no direct experimental evidence, such as a neutron diffraction experiment, for the existence of spontaneous magnetization in BBG. On the other hand, the models employed to investigate the gap include only several tight-binding parameters to describe the low-energy dispersions in the vicinity of the Dirac point [30,31,34]. Consequently, these models fail to capture the realistic behavior of the gap, exhibiting inconsistencies with experimental observations [30,31,34].

Therefore, it is necessary to investigate the behavior of the gap under an electric field based on a reasonable model to determine the ground state of BBG. Noticeably, some key ingredients such as interlayer van der Waals (VdW) interactions and ripples are often ignored by previous analyses. The interlayer VdW interactions and the ripples, which naturally occur in graphene sheets [43–45], are crucial to the properties of BBG since interlayer VdW interactions play a dominant

*yzzhang@tongji.edu.cn

role in anchoring the layers at a fixed distance [46] and ripples can drive graphene (including BBG consisting of two layers) into an insulator [47,48]. Furthermore, it has been suggested that a charge-ordered state, which may be favored by the two aforementioned ingredients in BBG, is possible in suspended graphene samples [49]. Thus, taking into account the effect of interlayer VdW interactions and ripples to provide a comprehensive explanation for the field-induced nonmonotonic behavior of the gap is an interesting work.

In this paper, we present a novel explanation for the phenomenon observed in BBG that the resistance varies nonmonotonically with an applied electric field, corresponding to the gap closing and then reopening with the electric field. We start by demonstrating the underlying physics of the phenomenon using a simple model with staggered potential between inequivalent sublattices on a Bernal-stacked bilayer honeycomb lattice. We reveal that the intrinsic gap at zero field is attributed to the presence of a particular intralayer charge-ordered state, which is characterized by an inverted order of the four low-energy bands, where two touched bands shift below the Fermi level while the other two untouched bands move above it [see Fig. 4(b)], in contrast to the disordered case, where touched ones meet at the Fermi level forming a massive Dirac cone [see Fig. 4(a)]. As an electric field is applied to this charge-ordered state, the upper band of the two touched bands and the lower band of the two untouched bands move towards and then cross each other, resulting in the nonmonotonic behavior of the gap at a small electric field. To validate the proposal that this charge-ordered state exists in BBG, we combine density functional theory (DFT) calculations with model analyses to include the effect of the interlayer van der Waals (VdW) interactions and ripples. We find that interlayer VdW interactions, along with ripples effectively generate a staggered potential between inequivalent sublattices in BBG. Most importantly, the experimental phenomenon is successfully reproduced when the strength of interlayer VdW interactions is on the order of 10 meV. Our results offer a fresh perspective on the field-induced intriguing phenomenon in BBG.

Our paper is structured as follows. In Sec. II, we provide a comprehensive description of the model and methods employed in our study. Section III presents our primary findings. Specifically, we calculate the gaps and intralayer charge disproportionations as functions of the staggered potential. We also examine how the eigenvalues of the Dirac point and low-energy bands vary when an electric field is applied. Additionally, we investigate the evolution of the gap with respect to the electric field when including the effect of interlayer VdW interactions and ripples. Section IV presents a detailed discussion, and Sec. V concludes our paper with a concise summary.

II. MODEL AND METHOD

The simple model that we employ to demonstrate the underlying physics for the intriguing phenomenon is given by

$$H = H_\tau + H_K + H_\Delta + H_E, \tag{1}$$

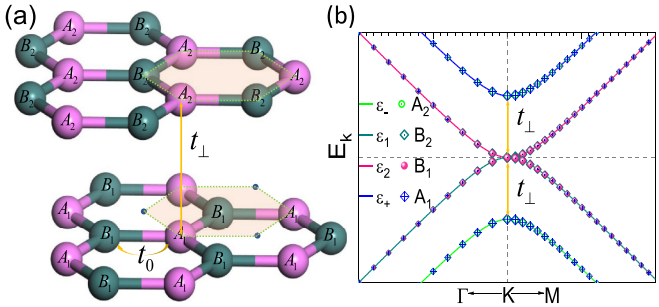

FIG. 1. (a) The structure of BBG, where the nearest intralayer and interlayer hoppings, namely, t_0 and $t_\perp$ are presented. (b) The low-energy bands of the disordered case, where $H_\Delta = 0$ and $H_E = 0$.

where

$$\begin{aligned}
H_K &= -t_0 \sum_{\langle ij\rangle\sigma} [C^\dagger_{iA_1\sigma} C_{jB_1\sigma} + C^\dagger_{iA_2\sigma} C_{jB_2\sigma}] + \text{H.c.},\\
H_\tau &= -t_\perp \sum_{i\sigma} C^\dagger_{iA_1\sigma} C_{iA_2\sigma} - t_\perp \sum_{i\sigma} C^\dagger_{iA_2\sigma} C_{iA_1\sigma},\\
H_\Delta &= \frac{1}{2}\Delta \sum_{i\sigma}\sum_m \hat{n}_{iA_m\sigma} - \frac{1}{2}\Delta \sum_{i\sigma}\sum_m \hat{n}_{iB_m\sigma},\\
H_E &= -\frac{1}{2} Eed \sum_{i\sigma}\sum_m (-1)^m [\hat{n}_{iA_m\sigma} + \hat{n}_{iB_m\sigma}].
\end{aligned} \tag{2}$$

Here, H_K, H_τ, H_Δ, and H_E denote the nearest intralayer hopping terms, the nearest interlayer hopping terms, staggered potential energy, and the external electric field terms, respectively. $C_{iS_m\sigma}$ annihilates an electron with spin σ on sublattice S (including A and B) of layer m in ith unit cell. $\hat{n}_{iS_m\sigma}$ is the particle-number operator. $\langle ij\rangle$ means summation over intralayer nearest-neighbor sites. t_0 and $t_\perp$ are hopping integrals as depicted in Fig. 1(a). Δ is the staggered potential with opposite signs in inequivalent sublattices, arising from distinct atomic environments of $A_{1(2)}$ and $B_{1(2)}$ sublattices, where A_2 is on top of A_1, whereas B_2 (B_1) is above (below) the center of the hexagon in the bottom (top) layer. A downward electric field E is studied. $d = 3.4$ Å is the interlayer distance, and e is the elementary charge. By applying Fourier transform, the Hamiltonian can be expressed in momentum space. Diagonalizing this Hamiltonian yields the eigenvalues of a given $\boldsymbol{k}$ point. Notably, the eigenvalues of the Dirac point are

$$\begin{aligned}
\varepsilon_1 &= -\frac{\Delta + eEd}{2}, \quad \varepsilon_- = \frac{\Delta}{2} - \sqrt{t_\perp^2 + \frac{(eEd)^2}{4}},\\
\varepsilon_2 &= \frac{eEd - \Delta}{2}, \quad \varepsilon_+ = \frac{\Delta}{2} + \sqrt{t_\perp^2 + \frac{(eEd)^2}{4}}.
\end{aligned} \tag{3}$$

It is easy to find that ε_1 and ε_2 are contributed by p_z orbitals of B_2 and B_1 atoms, respectively, whereas $\varepsilon_\pm$ are contributed by a linear combination of p_z orbitals of A_1 and A_2 atoms.

To accurately reproduce the intriguing phenomenon observed in BBG, it is imperative to include the effect of previously ignored interlayer VdW interactions and ripples. While ripples can be readily introduced through DFT calculations, the inclusion of interlayer VdW interactions is challenging due to the existence of various corrections such as vdW-DF [50], TS-vdW [51], vdW-DF-C [52], DFT-D [53],

etc. Thus, in order to gain insight into the effect of VdW interactions and eliminate the uncertainty from different choices of corrections, we construct a Hamiltonian as

$$H = H_D + H_{\text{eff}} + H_E, \tag{4}$$

where

$$H_D = -\sum_{is\sigma}\sum_{js'} t_{isjs'} C^{\dagger}_{is\sigma} C_{js'\sigma} \tag{5}$$

is the tight-binding Hamiltonian that describes the low-energy dispersion of DFT band structures, where the hopping parameters $t_{isjs'}$ can be derived through the transformation from Bloch space to maximally localized Wannier functions basis by using WANNIER90 code [54,55]. Four bands close to the Fermi energy, which are mainly contributed by p_z orbitals of four carbon sublattices, are taken into account. Sufficient numbers of long-range hoppings $t_{isjs'}$s are included in order to precisely describe the dispersion of low-energy bands obtained from DFT calculations as shown in Appendix A. The DFT band structures of BBG are calculated by the full-potential linearized augmented plane-wave method [56] within the density functional theory as implemented in the WIEN2K package [57], where the exchange-correlation interactions are treated by the local-density approximation [58]. A shifted $60 \times 60 \times 1$ special k-point mesh with a modified tetrahedron integration scheme [59] for the sampling of the Brillouin zone is employed. The valence and core states are separated by an energy of 6.0 Ry and the plane-wave cutoff parameter $R_{\text{mt}} \times k_{\text{max}}$ is set to be 7.00, where $R_{\text{mt}} = 1.33$ a.u. is used. The valence wave functions inside the atomic spheres are expanded up to $l_{\text{max}} = 10$ while the charge density is Fourier expanded up to $G_{\text{max}} = 12$. We choose both a charge convergence of 10^{-7}e and an energy convergence of 10^{-7} Ry as the convergence criteria. A sufficiently large vacuum distance of 17.1 Å is used to eliminate the interactions between periodic images of the layers in the direction perpendicular to the atomic plane. H_{eff} is the effective Hamiltonian capturing the effect of interlayer VdW interactions, and H_E is the aforementioned electric field terms. To obtain the effective Hamiltonian H_{eff}, we use a VdW potential of interatomic Lennard-Jones type

$$w_{ij}^{ss'} = V_0\left[\left(\frac{R_{ss'}}{|\boldsymbol{r}_{is} - \boldsymbol{r}_{js'}|}\right)^{12} - 2\left(\frac{R_{ss'}}{|\boldsymbol{r}_{is} - \boldsymbol{r}_{js'}|}\right)^{6}\right], \tag{6}$$

where $i(j)$ and $s(s')$ correspond to cell and sublattice indices, respectively. V_0 is the strength of interlayer VdW interactions, determining the depth of the potential well. $R_{ss'}$ represents the bottom of the sublattice-dependent interlayer VdW potential well, including R_{AA}, R_{BB}, R_{AB}, and R_{BA}. Since the interlayer VdW interactions play a dominant role in anchoring the layers at a fixed distance [46], $R_{ss'}$ can be approximated by force equilibrium condition of s sublattice in ith unit cell

$$12V_0 \sum_{j}{}' \left(\frac{R_{ss'}^6}{|\boldsymbol{r}_{is} - \boldsymbol{r}_{js'}|^7} - \frac{R_{ss'}^{12}}{|\boldsymbol{r}_{is} - \boldsymbol{r}_{js'}|^{13}}\right)\hat{\boldsymbol{e}}_{ij}^{ss'} = 0, \tag{7}$$

where $\hat{\boldsymbol{e}}_{ij}^{ss'} = (\boldsymbol{r}_{is} - \boldsymbol{r}_{js'})/|\boldsymbol{r}_{is} - \boldsymbol{r}_{js'}|$ is the unit vector, and $\sum'$ represents the summation over the layer without s sublattice. Thus, for a given V_0, the potential energy of s sublattices in ith unit cell reads

$$U_{is} = \frac{1}{2}V_0 \sum_{j}{}' \sum_{s'} w_{ij}^{ss'}. \tag{8}$$

Interestingly, there is a total potential energy difference between A-type and B-type sublattices as

$$\delta U_{AB} = \sum_{i}(U_{iA_1} + U_{iA_2} - U_{iB_1} - U_{iB_2}), \tag{9}$$

namely, the potential energy well of $A_{1(2)}$ is higher than that of $B_{1(2)}$. As a result, electrons redistribute in response to eliminate this difference compared with the case without the interlayer VdW interactions. Thus, interlayer VdW interactions effectively generate a staggered potential between inequivalent sublattices in the layer, namely, H_{eff} satisfies

$$H_{\text{eff}} = \Delta \sum_{i\sigma}\sum_{m}[\hat{n}_{iA_m\sigma} - \hat{n}_{iB_m\sigma}]/2,$$
$$\delta U_{AB} = -\langle H_{\text{eff}}\rangle. \tag{10}$$

Thus, the staggered potential is determined as long as the strength of interlayer VdW interactions V_0 is given.

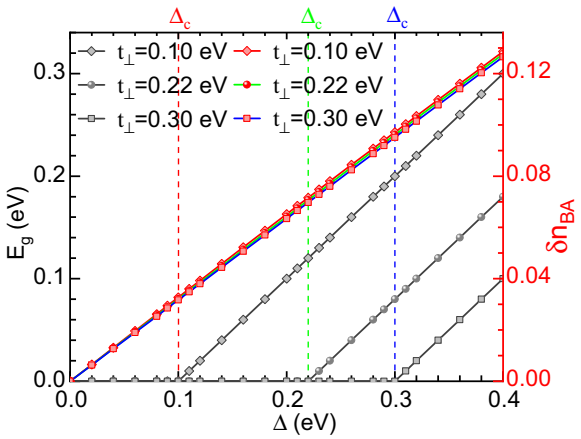

FIG. 2. The gaps E_g and intralayer charge disproportionation δn_{BA} as functions of staggered potential Δ for three nearest interlayer coupling with $t_\perp = 0.1$ eV, $t_\perp = 0.22$ eV, and $t_\perp = 0.3$ eV. $t_0 = 2.7$ eV is used here. Gray symbols and left axis describe the band gap while red symbols and right axis depict the charge disproportionation δn_{BA}.

III. RESULTS

Here, we demonstrate first the underlying physics for the phenomenon that the gap closes and then reopens with the electric field using the simple model (1) as introduced above. Starting with the insulating state at zero field ($E = 0$), we find that the intrinsic gap at zero field is due to the presence of a particular intralayer charge-ordered state where sublattice B is charge rich while sublattice A is charge poor. To illustrate this, we calculate the gaps E_g and intralayer charge disproportionation (CD) $\delta n_{BA} = \frac{1}{2}(n_{B_1} + n_{B_2} - n_{A_1} - n_{A_2})$ as functions of the staggered potential Δ for different interlayer couplings $t_\perp$ at zero field, as shown in Fig. 2. As can be seen, the model always predicts a charge-ordered insulating state when $\Delta > \Delta_c$ despite the differences in $t_\perp$. This insulating state can

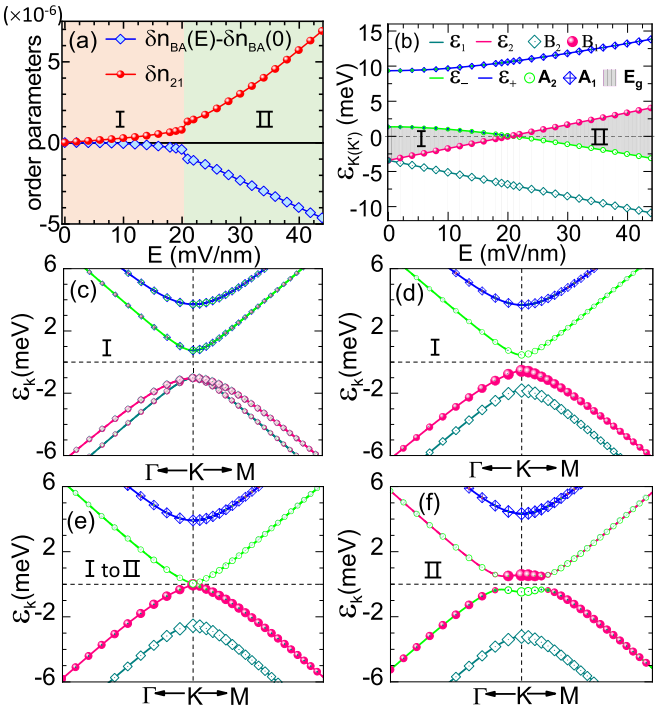

FIG. 3. (a) δn_{21} and $\delta n_{BA}(E) - \delta n_{BA}(0)$ as functions of the electric field, where δn_{21}, $\delta n_{BA}(E)$, and $\delta n_{BA}(0)$ are the order parameters of interlayer CD, field-dependent intralayer CD, and zero-field intralayer CD, respectively. (b) The field-dependent eigenvalues at the Dirac point. (c)–(f) present the evolution of low-energy bands with respect to the electric field, including $E = 0$ mV/nm (a), 10 mV/nm (b), 20 mV/nm (c), and 30 mV/nm (d). To show all of the low-energy bands within the same energy scale, we use $t_\perp = 4$ meV, $t_0 = 2.7$ eV, $\Delta = 8.8$ meV here.

be understood using the eigenvalues of Dirac point [Eq. (3)] since they are relevant to the low-energy bands at half-filling. We find that when $\Delta \leqslant t_\perp$, the system remains metallic as the Fermi level lies between the degenerate eigenvalues ε_1 and ε_2. In contrast, when $\Delta > t_\perp$, ε_- and $\varepsilon_1(\varepsilon_2)$ are inverted compared with the disordered case [see Figs. 1(b) and 3(c)], resulting in a band-inverted charge-ordered insulating state with a gap of $E_g = \Delta - t_\perp$. The latter may be relevant to the zero-field insulating state observed in BBG. For example, $t_\perp \approx 0.22$ eV [24] in BBG, a weakly intralayer CD with critical $\delta n_{BA} \approx 0.07$ can make it an insulator (Fig. 2). Since a reduced threefold symmetry characteristic is observed by high-resolution scanning tunneling microscopy [43], implying an intralayer CD, we argue that the insulating state of BBG at zero field is probably due to the presence of this band-inverted intralayer charge-ordered state.

Proceeding to analyze the effect of an electric field E on the band-inverted charge-ordered insulating state, we find that the gap decreases for $E < E_c$, increases for $E > E_c$, with the gap closing at critical value $E = E_c$, which is reminiscent of the intriguing phenomenon observed experimentally that resistance varies nonmonotonically with an electric field [26]. A downward electric field can drive the electrons from the bottom to the top layers, resulting in interlayer CD. Figure 3(a) shows δn_{21} and $\delta n_{BA}(E) - \delta n_{BA}(0)$ as functions of the electric

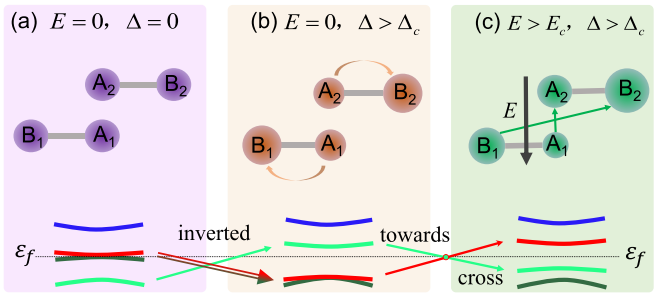

FIG. 4. The charge distribution and bands in the vicinity of the Dirac point for different cases with (a) absence of electric field and staggered potential, (b) staggered potential is larger than the critical value but without an electric field, (c) both electric field and staggered potential are larger than the critical value. The size of the ball represents the charge population in corresponding site.

field, where $\delta n_{21} = n_{A_2} + n_{B_2} - n_{A_1} - n_{B_1}$ is the order parameter of the interlayer CD while $\delta n_{BA}(E)$ and $\delta n_{BA}(0) \approx 5.84512 \times 10^{-3}$ are the order parameters of the field-dependent and zero-field intralayer CDs, respectively. Noticeably, as the band gap is relatively small, we have chosen $t_\perp$ and Δ comparable to the band gap to clearly demonstrate the detailed evolution of all four relevant low-energy bands with the small electric field, which does not alter the underlying physics. As can be seen, distinct behaviors of δn_{21} and $\delta n_{BA}(E) - \delta n_{BA}(0)$ in $E < E_c$ and $E > E_c$ imply a phase transition from phase I to II at $E = E_c$. As a small electric field mainly affects the low-energy bands of the system, the phase transition can also be understood using the eigenvalues of the Dirac point. Figure 3(b) shows the eigenvalues of the Dirac point varying with the electric field. We find ε_2 and ε_+ raise up, whereas ε_1 and ε_- go down with the increase of the electric field. This is because ε_2, ε_+, ε_1, and ε_- are mainly contributed by p_z orbitals of B_1, A_1, B_2, and A_2 sites, respectively, where the on-site potentials of B_1 and A_1 sites increase, whereas those of B_2 and A_2 sites decrease when an electric field is applied. Given that ε_- is higher than ε_2 at $E = 0$, ε_- and ε_2 will move towards and then cross each other as shown in Figs. 3(c)–3(f) [or in Figs. 4(b) and 4(c)]. Consequently, the gap decreases for $E < E_c$ and increases for $E > E_c$. Notably, the gap closes at the critical electric field $E_c = (\Delta^2 - t_\perp^2)/(ed\Delta)$. Thus, the gap of the band-inverted intralayer charge-ordered insulating state varies nonmonotonously with the electric field.

In brief, the findings above can be summarized as a schematic illustration in Fig. 4, demonstrating the following physics. (i) An intralayer charge-ordered state can open an intrinsic gap in the BBG lattice at zero field when band inversion between the two touched bands and the lower band of the two untouched bands occurs, compared with the disordered case [see Figs. 4(b) and 4(a)]. (ii) When an electric field is applied to this charge-ordered insulating state, the upper band of the two touched bands and the lower band of the two untouched bands move towards and then cross each other as shown from Figs. 4(b)–4(c), resulting in a nonmonotonic behavior of the gap that closes and then reopens with the electric field. As we proposed in Sec. II that the interlayer VdW interactions can effectively generate a staggered potential between intralayer inequivalent sublattices. Besides, the ripples, which naturally

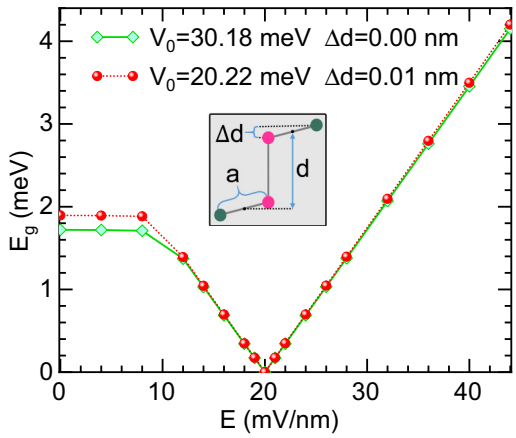

FIG. 5. The gaps of flat and rippled structures as functions of the electric field. $d = 0.34$ nm and $a = 0.142$ nm are used. $\Delta d = 0.01$ nm in rippled structure which is presented in inset.

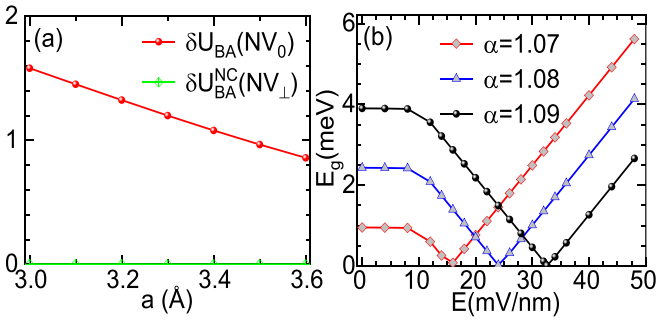

FIG. 6. (a) The potential energy differences between inequivalent sublattices generated individually by the interlayer Coulomb interactions (δU_{BA}^{NC}) and that generated individually by the interlayer VdW interactions (δU_{BA}) for the flat structure as functions of interlayer distance d, where V_0 is the strength of the interlayer VdW interactions and $V_\perp$ is the strength of the nearest-neighbor interlayer Coulomb interaction. $V(r) = V_\perp \frac{d}{r}$ is used for the interlayer Coulomb interactions. N is the number of unit cells. (b) The calculated band gap of model (4) as functions of the electric field, where the Kolmogorov-Crespi potential is used to derive H_{eff} and α is the correction factor for the repulsive term of the Kolmogorov-Crespi potential in BBG as introduced in Appendix B.

exist in BBG, may favor a charge-ordered state. Thus, this band-inverted intralayer charge-ordered insulating state may be the key to the nonmonotonic resistance phenomenon observed in BBG, and it is imperative to study the effect of previously ignored interlayer VdW interactions and ripples.

To validate our proposal that the intriguing phenomenon observed in BBG is due to the presence of the aforementioned band-inverted charge-ordered state, the model presented in Sec. II, specifically Eq. (4), which includes the effect of interlayer VdW interactions and ripples, is employed to calculate the gap of BBG. For a given strength of interlayer VdW interactions V_0, the effective Hamiltonian H_{eff}, especially the staggered potential Δ, should be self-consistently determined. Thus, we derive first the potential energy difference between A and B sublattices using the method presented in Sec. II. We find $\delta U_{AB} \approx 1.08 N V_0$ and $\delta U_{AB} \approx 2.08 N V_0$ for flat structure and Peierls-type rippled structure with $\Delta d = 0.01$ nm, respectively, where N is the number of unit cells. Using Eq. (10), the effective staggered potential is calculated as $\Delta = \delta U_{AB}/(N \delta n_{BA})$. Thus, δn_{BA} and Δ are self-consistently determined by combining this equation with Eq. (4) as long as V_0 is given, indicating that H_{eff} can be determined self-consistently. Therefore, the gaps and CDs of bilayer graphene for a given strength of interlayer VdW interactions are calculated. Figure 5 shows the gaps of BBG as functions of the electric field for flat and rippled structures with the strength of interlayer VdW interactions of $V_0 = 30.18$ meV and $V_0 = 20.22$ meV, respectively, where the gap decreases for $E < E_c$, increases for $E > E_c$, with the closure of the gap at $E_c = 20$ mV/nm. As the resistance $R \propto \exp[E_g/(k_B T)]$, our results are in excellent agreement with the experimental phenomenon that the resistance decreases and then increases with the electric field, where minimal resistance is at critical electric field $E_c \approx 20$ mV/nm [26] and the zero-field gap is $E_g \approx 2$ meV [27,28,60,61]. It is necessary to mention that a weakly spontaneous charge-ordered state occurs for both cases with intralayer CD $\delta n_{BA} = 0.10 \sim 0.12$, where δn_{BA} changes very little with the electric field while δn_{21} increases from 0 to 3×10^{-4}. In addition, a smaller V_0 can lead to the same behavior of gap for the rippled structure compared with the flat case, suggesting that the ripple concerned and interlayer VdW interactions are cooperative. Thus, interlayer VdW interactions cooperating with ripples can effectively generate a staggered potential between inequivalent sublattices, which induces an intralayer charge-ordered insulating state, resulting in the experimental phenomenon observed in BBG. The strength of the interlayer VdW interactions is of the order of 10 meV. Please note that $R_{ss'}$s are not tunable parameters, which are determined by the force equilibrium condition. The critical values of V_0 that cause the metal-to-insulator phase transitions at zero field for flat and ripple structures are 29.85 meV and 20.00 meV, respectively.

IV. DISCUSSION

Here, a simple model has been used to demonstrate the underlying physics for the intriguing phenomenon observed in BBG that the resistance decreases and then increases with the electric field at low temperatures. We ascribe this phenomenon to the presence of a band-inverted charge-ordered insulating state in BBG. Our proposal is further confirmed by combining DFT calculations with model calculations, where we take into account the effect of the interlayer VdW interactions and ripples. Our results are reliable because our calculations include not only the effects of the nonlocal Coulomb interactions and remote hoppings at the DFT level but also the previously ignored ingredients, namely interlayer VdW interactions and ripple in the layer. Noticeably, although the interlayer Coulomb interactions are stronger than the interlayer VdW interactions, the potential difference between inequivalent sublattices generated by the interlayer Coulomb interactions is much smaller than that generated by the interlayer VdW interactions as presented in Fig. 6(a). Thus, the interlayer VdW interactions play a major role in determining the intralayer charge-ordered state of BBG. However, this key ingredient is often ignored by previous studies.

The validity of modeling BBG by a bilayer honeycomb lattice with staggered potentials is as follows: Although DFT can provide a reasonable energy difference between AA-stacking bilayer graphene and BBG due to cancellation of the uncertainty from interlayer interactions simultaneously [62], it fails to capture the interlayer interactions for each structure individually. Therefore, it is necessary to model the uncertainty arising from interlayer interactions, which may induce a staggered potential between $A_{1(2)}$ and $B_{1(2)}$ sublattices due to their inequivalent interlayer environment. Indeed, our results suggest the presence of a staggered potential due to the interlayer interactions, e.g., VdW interactions. The calculated small band gap, which is consistent with the experimental observations in bilayer graphene devices [27,28,60,61], strongly indicates that the system is in the critical region of insulator-to-metal transition.

Although varieties of corrections such as vdW-DF [50], TS-vdW [51], vdW-DF-C [52], DFT-D [53], and so on have been proposed, the electronic properties of the BBG and graphite obtained from these corrections are diverse from each other [63,64]. Thus, in order to gain insight into the effect of VdW interactions and eliminate the uncertainty from different choices of corrections, it is necessary to treat the interlayer VdW interactions as free parameters, namely modeling the effect of interlayer VdW interactions. In our calculations, the model Hamiltonian for interlayer VdW interactions is obtained naturally from the interatomic Lennard-Jones potential, where the strength of interlayer VdW interactions V_0 serves as the sole free parameter except for the electric field in Eq. (4). Noticeably, the isotropic nature of the Lennard-Jones VdW potential can not capture the anisotropic properties of BBG. Thus, we also employ the Kolmogorov-Crespi potential [62] to take into account the interlayer interactions with anisotropy as introduced in Appendix B. Similar behavior that the band gap varies nonmonotonically with the electric field has also been observed as shown in Fig. 6(b).

Although several correlated symmetry-broken gapped states with parabolic dispersion relation have been proposed at zero field, namely LAF, CAF, QAH, and QSH, the low-energy bands of BBG observed experimentally at a small applied magnetic field cannot be explained within the framework of parabolic bands, which predicts roughly equidistant Landau levels at low temperatures [65]. Besides, there is a pronounced asymmetry in the cyclotron mass between hole and electron doping [24]. These findings raise doubts about the candidates that exhibit a parabolic dispersion relation with particle-hole symmetry near the Fermi level. Moreover, as the temperature increases from zero, two resistance transitions occur. One transition is observed at $\sim$12 K [66], while the other occurs at 200 $\sim$ 250 K [67], which is suggested to be caused by the interlayer ripple scattering effect. As the charge-ordered state we proposed still exists even when the gap is closed, it may suggest that the former transition corresponds to the evolution from the charge-ordered insulating state to the charge-ordered metallic state, while the latter transition corresponds to the change from the charge-ordered metallic state to the disordered state.

Ripples are inherent features of BBG, arising from the natural undulations of suspended graphene sheets. It has been proposed that suspended graphene sheets are not perfectly flat showing ripples with an amplitude of about 1 nm [43–45] with dislocations [68]. Here, for simplicity, we take the Peierls-type ripple into account, which is energetically favored by elastic effects [69]. However, it should be noted that the ripples in BBG exhibit a complex nature. Thus, it is interesting to study how the experimentally observed ripples cooperate with interlayer VdW interactions to affect the properties of the intralayer charge-ordered state.

Although the charge-ordered state we studied has been previously investigated [70], the properties of this charge-ordered state under an external field have not been explored before. Noticeably, a low-energy theory based on a 2×2 Hamiltonian matrix with consideration of the charge-ordered characteristic is used to study the properties of BBG [36]. However, it fails to deal with the properties of the charge-ordered state concerned here, where the low-energy bands are inverted. Besides, although low-energy theory based on a 4×4 Hamiltonian matrix is also proposed, it does not take into account the effect of a charge-ordered state [23,71].

Here, we study the phenomenon observed in BBG that the gap varies nonmonotonously with the electric field. Our results strongly suggest that the ground state of BBG is a charge-ordered insulating state. Therefore, further experiments are needed to confirm the ground state of BBG. There are two experimental approaches to identify this state: one is angle-resolved photoelectron spectroscopy and the other is scanning tunneling spectroscopy. An experiment based on angular-resolved photoemission spectroscopy should be done at low temperatures, without external perturbations, to detect the low-energy bands of BBG. If the low-energy bands are inverted, the ground state of BBG is a charge-ordered state. Alternatively, the scanning tunneling spectroscopy would be sensitive to the charge ordering at atomic scale, allowing one to measure spatial variations of the local density of states to determine the ground state of BBG.

V. CONCLUSION

In conclusion, an intriguing phenomenon that the resistance varies nonmonotonously with an electric field applied perpendicular to the plane has been observed at low temperatures in BBG. Here, we suggest that this phenomenon is probably due to the presence of a spontaneous charge-ordered insulating state in BBG. The underlying physics is illustrated by a simple model on BBG lattice with staggered potential between inequivalent sublattices. To validate our proposal, we combine DFT calculations with model calculations to include the effect of the interlayer VdW interactions and ripples. We find that the interlayer VdW interactions cooperating with ripples can effectively generate a staggered potential in BBG. Remarkably, we have successfully reproduced the gap amplitude and the critical electric field when the strength of the interlayer VdW interactions is on the order of 10 meV. Our results provide a new perspective on the nonmonotonic resistance phenomenon in BBG and suggest that the ground state of BBG is likely a charge-ordered state. We argue that angular-resolved photoemission spectroscopy studies at zero field or scanning tunneling spectroscopy can be used to identify the ground state at low temperatures.

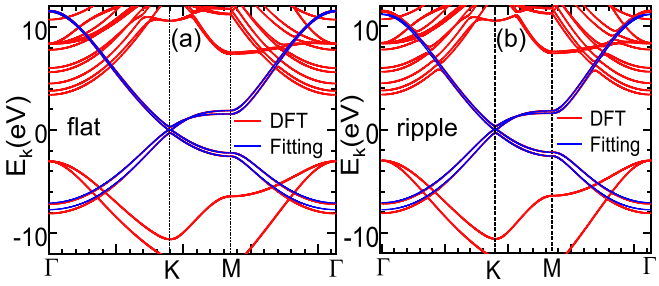

FIG. 7. The bands obtained from DFT calculations and the corresponding Wannier fittings (a) for flat structure and (b) for ripple structure with $\Delta d = 0.01$ nm.

ACKNOWLEDGMENTS

This work is supported by National Natural Science Foundation of China (Grants No. 12274324 and No. 12004283) and Shanghai Science and Technology Commission (Grant No. 21JC405700).

APPENDIX A: WANNIER FITTINGS TO THE LOW-ENERGY DFT BANDS

Due to the fact that only including t_0 and $t_\perp$ is not sufficient to well describe the low-energy DFT bands of BBG, we establish a tight-binding model H_D with long-range hoppings to accurately describe the entire dispersions of low-energy DFT bands. For both flat and ripple structures, the fitted bands provided by the tight-binding Hamiltonian of all p_z orbitals (blue) and DFT bands (red) match well as shown in Fig. 7.

APPENDIX B: TOTAL POTENTIAL ENERGY DIFFERENCE BETWEEN A-TYPE AND B-TYPE SUBLATTICES DERIVED FROM THE KOLMOGOROV-CRESPI POTENTIAL

It has been pointed out that the isotropic nature of the Lennard-Jones VdW potential can not capture the anisotropic properties of the graphitic systems. Then, Kolmogorov and Crespi take into account the in-plane and out-of-plane anisotropy, proposing the so-called Kolmogorov-Crespi potential to describe the interlayer interactions in graphite systems [62]. The interatomic Kolmogorov-Crespi potential depicting the graphitic systems reads

$$w_{ij}^{ss'} = e^{-\lambda(r_{is}^{js'}-d)}\left[C + f\left(\rho_{is}^{js'}\right) + f\left(\rho_{js'}^{is}\right)\right] - A\left(\frac{r_{is}^{js'}}{d}\right)^6, \tag{B1}$$

with

$$\begin{aligned} r_{is}^{js'} &= |\boldsymbol{r_{is}} - \boldsymbol{r_{js'}}|, \\ \left(\rho_{is}^{js'}\right)^2 &= \left(r_{is}^{js'}\right)^2 - \left(\boldsymbol{n_{is}} \cdot \boldsymbol{r}_{is}^{js'}\right)^2, \\ \left(\rho_{js'}^{is}\right)^2 &= \left(r_{js'}^{is}\right)^2 - \left(\boldsymbol{n_{js'}} \cdot \boldsymbol{r}_{js'}^{is}\right)^2, \\ f\left(\rho_{is}^{js'}\right) &= e^{-\rho_{is}^{js'}/\delta} \sum_{n=0}^{2} C_{2n} \left(\rho_{is}^{js'}/\delta\right)^{2n}, \end{aligned} \tag{B2}$$

where d is the interlayer distance while the other constants are as follows:

$$\begin{aligned} &C_0 = 15.71\,\text{meV} \quad C_2 = 12.29\,\text{meV} \\ &C_4 = 4.933\,\text{meV} \quad C = 3.030\,\text{meV} \\ &\delta = 0.578\,\text{Å} \quad \lambda = 3.629\,\text{Å}^{-1} \quad A = 10.238\,\text{meV}. \end{aligned} \tag{B3}$$

Besides, it was shown that for a layered system composed of two monolayer planes such as BBG, the Casimir force plays a significant role in phase transitions [72]. As the Casimir force generates an additional attractive interaction between the two planes, the repulsive term of the Kolmogorov-Crespi potential for BBG has to be larger than that of graphite. Thus, the interatomic Kolmogorov-Crespi potential describing BBG can be written as

$$w_{ij}^{ss'} = \alpha e^{-\lambda(r_{is}^{js'}-d)}\left[C + f\left(\rho_{is}^{js'}\right) + f\left(\rho_{js'}^{is}\right)\right] - A\left(\frac{r_{is}^{js'}}{d}\right)^6, \tag{B4}$$

where α is the correction factor for the repulsive term of the Kolmogorov-Crespi potential in BBG, which should be slightly larger than 1 and the other constants remain the same as those of graphite. Substituting this equation into Eq. (8) can determine the staggered potentials and consequently calculate the band gap of BBG once α is given by applying Eqs. (4), (9), and (10) subsequently. The calculated band gap of BBG under the applied electric field is shown in Fig. 6(b), which qualitatively agrees with the result shown in Fig. 5 where the Lennard-Jones VdW potential is used.

[1] K. S. Novoselov, E. McCann, S. V. Morozov, V. I. Fal'ko, M. I. Katsnelson, U. Zeitler, D. Jiang, F. Schedin, and A. K. Geim, Unconventional quantum Hall effect and Berry's phase of 2π in bilayer graphene, Nat. Phys. **2**, 177 (2006).

[2] A. Kou, B. E. Feldman, A. J. Levin, B. I. Halperin, K. Watanabe, T. Taniguchi, and A. Yacoby, Electron-hole asymmetric integer and fractional quantum Hall effect in bilayer graphene, Science **345**, 55 (2014).

[3] Y. Cao, V. Fatemi, S. Fang, K. Watanabe, T. Taniguchi, E. Kaxiras, and P. Jarillo-Herrero, Unconventional superconductivity in magic-angle graphene superlattices, Nature (London) **556**, 43 (2018).

[4] X. Lu, P. Stepanov, W. Yang, M. Xie, M. A. Aamir, I. Das, C. Urgell, K. Watanabe, T. Taniguchi, G. Zhang *et al.*, Superconductors, orbital magnets and correlated states in magic-angle bilayer graphene, Nature (London) **574**, 653 (2019).

[5] M. J. Park, Y. Kim, G. Y. Cho, and S. Lee, Higher-order topological insulator in twisted bilayer graphene, Phys. Rev. Lett. **123**, 216803 (2019).

[6] C.-H. Park and S. G. Louie, Tunable excitons in biased bilayer graphene, Nano Lett. **10**, 426 (2010).

[7] L. Ju, L. Wang, T. Cao, T. Taniguchi, K. Watanabe, S. G. Louie, F. Rana, J. Park, J. Hone, F. Wang *et al.*, Tunable excitons in bilayer graphene, Science **358**, 907 (2017).

[8] M. Sui, G. Chen, L. Ma, W.-Y. Shan, D. Tian, K. Watanabe, T. Taniguchi, X. Jin, W. Yao, D. Xiao *et al.*, Gate-tunable topological valley transport in bilayer graphene, Nat. Phys. **11**, 1027 (2015).

[9] A. V. Rozhkov, A. O. Sboychakov, A. L. Rakhmanov, and F. Nori, Electronic properties of graphene-based bilayer systems, Phys. Rep. **648**, 1 (2016).

[10] J. B. Oostinga, H. B. Heersche, X. Liu, A. F. Morpurgo, and L. M. K. Vandersypen, Gate-induced insulating state in bilayer graphene devices, Nat. Mater. **7**, 151 (2008).

[11] B. E. Feldman, J. Martin, and A. Yacoby, Broken-symmetry states and divergent resistance in suspended bilayer graphene, Nat. Phys. **5**, 889 (2009).

[12] T. Taychatanapat and P. Jarillo-Herrero, Electronic transport in dual-gated bilayer graphene at large displacement fields, Phys. Rev. Lett. **105**, 166601 (2010).

[13] P. Maher, C. R. Dean, A. F. Young, T. Taniguchi, K. Watanabe, K. L. Shepard, J. Hone, and P. Kim, Evidence for a spin phase transition at charge neutrality in bilayer graphene, Nat. Phys. **9**, 154 (2013).

[14] J. Li, H. Fu, Z. Yin, K. Watanabe, T. Taniguchi, and J. Zhu, Metallic phase and temperature dependence of the $\nu = 0$ quantum Hall state in bilayer graphene, Phys. Rev. Lett. **122**, 097701 (2019).

[15] T. Ohta, A. Bostwick, T. Seyller, K. Horn, and E. Rotenberg, Controlling the electronic structure of bilayer graphene, Science **313**, 951 (2006).

[16] J. Park, S. B. Jo, Y.-J. Yu, Y. Kim, J. W. Yang, W. H. Lee, H. H. Kim, B. H. Hong, P. Kim, K. Cho *et al.*, Single-gate bandgap opening of bilayer graphene by dual molecular doping, Adv. Mater. **24**, 407 (2012).

[17] E. J. Mele, Commensuration and interlayer coherence in twisted bilayer graphene, Phys. Rev. B **81**, 161405(R) (2010).

[18] S. Shallcross, S. Sharma, E. Kandelaki, and O. A. Pankratov, Electronic structure of turbostratic graphene, Phys. Rev. B **81**, 165105 (2010).

[19] Y. Cao, V. Fatemi, A. Demir, S. Fang, S. L. Tomarken, J. Y. Luo, J. D. Sanchez-Yamagishi, K. Watanabe, T. Taniguchi, E. Kaxiras *et al.*, Correlated insulator behaviour at half-filling in magic-angle graphene superlattices, Nature (London) **556**, 80 (2018).

[20] Y. Zhang, T.-T. Tang, C. Girit, Z. Hao, M. C. Martin, A. Zettl, M. F. Crommie, Y. R. Shen, and F. Wang, Direct observation of a widely tunable bandgap in bilayer graphene, Nature (London) **459**, 820 (2009).

[21] K. F. Mak, C. H. Lui, J. Shan, and T. F. Heinz, Observation of an electric-field-induced band gap in bilayer graphene by infrared spectroscopy, Phys. Rev. Lett. **102**, 256405 (2009).

[22] E. McCann, D. S. L. Abergel, and V. I. Fal'ko, The low energy electronic band structure of bilayer graphene, Eur. Phys. J.: Spec. Top. **148**, 91 (2007).

[23] E. McCann, Asymmetry gap in the electronic band structure of bilayer graphene, Phys. Rev. B **74**, 161403(R) (2006).

[24] E. V. Castro, K. S. Novoselov, S. V. Morozov, N. M. R. Peres, J. M. B. Lopes dos Santos, J. Nilsson, F. Guinea, A. K. Geim, and A. H. Castro Neto, Biased bilayer graphene: Semiconductor with a gap tunable by the electric field effect, Phys. Rev. Lett. **99**, 216802 (2007).

[25] E. McCann and M. Koshino, The electronic properties of bilayer graphene, Rep. Prog. Phys. **76**, 056503 (2013).

[26] R. T. Weitz, M. T. Allen, B. E. Feldman, J. Martin, and A. Yacoby, Broken-symmetry states in doubly gated suspended bilayer graphene, Science **330**, 812 (2010).

[27] W. Bao, J. Velasco, F. Zhang, L. Jing, B. Standley, D. Smirnov, M. Bockrath, A. H. MacDonald, and C. N. Lau, Evidence for a spontaneous gapped state in ultraclean bilayer graphene, Proc. Natl. Acad. Sci. USA **109**, 10802 (2012).

[28] J. Velasco, L. Jing, W. Bao, Y. Lee, P. Kratz, V. Aji, M. Bockrath, C. N. Lau, C. Varma, R. Stillwell *et al.*, Transport spectroscopy of symmetry-broken insulating states in bilayer graphene, Nat. Nanotechnol. **7**, 156 (2012).

[29] T. C. Lang, Z. Y. Meng, M. M. Scherer, S. Uebelacker, F. F. Assaad, A. Muramatsu, C. Honerkamp, and S. Wessel, Antiferromagnetism in the Hubbard model on the Bernal-stacked honeycomb bilayer, Phys. Rev. Lett. **109**, 126402 (2012).

[30] J. Yuan, D.-H. Xu, H. Wang, Y. Zhou, J.-H. Gao, and F.-C. Zhang, Possible half-metallic phase in bilayer graphene: Calculations based on mean-field theory applied to a two-layer Hubbard model, Phys. Rev. B **88**, 201109(R) (2013).

[31] J. Jung, F. Zhang, and A. H. MacDonald, Lattice theory of pseudospin ferromagnetism in bilayer graphene: Competing interaction-induced quantum Hall states, Phys. Rev. B **83**, 115408 (2011).

[32] Y. Wang, H. Wang, J.-H. Gao, and F.-C. Zhang, Layer antiferromagnetic state in bilayer graphene: A first-principles investigation, Phys. Rev. B **87**, 195413 (2013).

[33] M. M. Scherer, S. Uebelacker, and C. Honerkamp, Instabilities of interacting electrons on the honeycomb bilayer, Phys. Rev. B **85**, 235408 (2012).

[34] M. Kharitonov, Canted antiferromagnetic phase of the $\nu = 0$ quantum Hall state in bilayer graphene, Phys. Rev. Lett. **109**, 046803 (2012).

[35] Y. Lemonik, I. Aleiner, and V. I. Fal'Ko, Competing nematic, antiferromagnetic, and spin-flux orders in the ground state of bilayer graphene, Phys. Rev. B **85**, 245451 (2012).

[36] R. Nandkishore and L. Levitov, Quantum anomalous Hall state in bilayer graphene, Phys. Rev. B **82**, 115124 (2010).

[37] S. Ray and L. Janssen, Gross-Neveu-Heisenberg criticality from competing nematic and antiferromagnetic orders in bilayer graphene, Phys. Rev. B **104**, 045101 (2021).

[38] J.-R. Xu, Z.-Y. Song, H.-Q. Lin, and Y.-Z. Zhang, Gate-induced gap in bilayer graphene suppressed by Coulomb repulsion, Phys. Rev. B **93**, 035109 (2016).

[39] V. Cvetkovic, R. E. Throckmorton, and O. Vafek, Electronic multicriticality in bilayer graphene, Phys. Rev. B **86**, 075467 (2012).

[40] R. E. Throckmorton and O. Vafek, Fermions on bilayer graphene: Symmetry breaking for $b = 0$ and $\nu = 0$, Phys. Rev. B **86**, 115447 (2012).

[41] A. L. Szabó and B. Roy, Extended Hubbard model in undoped and doped monolayer and bilayer graphene: Selection rules and organizing principle among competing orders, Phys. Rev. B **103**, 205135 (2021).

[42] F. Zhang, J. Jung, G. A. Fiete, Q. Niu, and A. H. MacDonald, Spontaneous quantum Hall states in chirally stacked few-layer graphene systems, Phys. Rev. Lett. **106**, 156801 (2011).

[43] E. Stolyarova, K. T. Rim, S. Ryu, J. Maultzsch, P. Kim, L. E. Brus, T. F. Heinz, M. S. Hybertsen, and G. W. Flynn, High-resolution scanning tunneling microscopy imaging of

mesoscopic graphene sheets on an insulating surface, Proc. Natl. Acad. Sci. USA **104**, 9209 (2007).
[44] J. C. Meyer, A. K. Geim, M. I. Katsnelson, K. S. Novoselov, T. J. Booth, and S. Roth, The structure of suspended graphene sheets, Nature (London) **446**, 60 (2007).
[45] A. Fasolino, J. H. Los, and M. I. Katsnelson, Intrinsic ripples in graphene, Nat. Mater. **6**, 858 (2007).
[46] F. Zhang, B. Sahu, H. Min, and A. H. MacDonald, Band structure of ABC-stacked graphene trilayers, Phys. Rev. B **82**, 035409 (2010).
[47] G. Gui, J. Zhong, and Z. Ma, Electronic properties of rippled graphene, *Journal of Physics: Conference Series* (IOP Publishing, Bristol, 2012), Vol. 402, p. 012004.
[48] S.-Y. Lin, S.-L. Chang, F.-L. Shyu, J.-M. Lu, and M.-F. Lin, Feature-rich electronic properties in graphene ripples, Carbon **86**, 207 (2015).
[49] J. Jung and A. H. MacDonald, Theory of the magnetic-field-induced insulator in neutral graphene sheets, Phys. Rev. B **80**, 235417 (2009).
[50] M. Dion, H. Rydberg, E. Schröder, D. C. Langreth, and B. I. Lundqvist, Van der Waals density functional for general geometries, Phys. Rev. Lett. **92**, 246401 (2004).
[51] A. Tkatchenko and M. Scheffler, Accurate molecular van der Waals interactions from ground-state electron density and free-atom reference data, Phys. Rev. Lett. **102**, 073005 (2009).
[52] V. R. Cooper, Van der Waals density functional: An appropriate exchange functional, Phys. Rev. B **81**, 161104(R) (2010).
[53] S. Grimme, J. Antony, S. Ehrlich, and H. Krieg, A consistent and accurate *ab initio* parametrization of density functional dispersion correction (DFT-D) for the 94 elements H-Pu, J. Chem. Phys. **132**, 154104 (2010).
[54] N. Marzari, A. A. Mostofi, J. R. Yates, I. Souza, and D. Vanderbilt, Maximally localized Wannier functions: Theory and applications, Rev. Mod. Phys. **84**, 1419 (2012).
[55] A. A. Mostofi, J. R. Yates, Y.-S. Lee, I. Souza, D. Vanderbilt, and N. Marzari, WANNIER90: A tool for obtaining maximally-localised Wannier functions, Comput. Phys. Commun. **178**, 685 (2008).
[56] D. J. Singh and L. Nordstrom, *Planewaves, Pseudopotentials, and the LAPW method* (Springer, Berlin, 2006).
[57] P. Blaha, K. Schwarz, G. Madsen, D. Kvasnicka, and J. Luitz, *WIEN2k, An Augmented Plane Wave+Local Orbitals Program for Calculating Crystal Properties* (K. Schwarz, Technische Universität Wien, Austria, 2001).
[58] J. P. Perdew and A. Zunger, Self-interaction correction to density-functional approximations for many-electron systems, Phys. Rev. B **23**, 5048 (1981).
[59] P. E. Blöchl, O. Jepsen, and O. K. Andersen, Improved tetrahedron method for Brillouin-zone integrations, Phys. Rev. B **49**, 16223 (1994).
[60] F. Freitag, J. Trbovic, M. Weiss, and C. Schönenberger, Spontaneously gapped ground state in suspended bilayer graphene, Phys. Rev. Lett. **108**, 076602 (2012).
[61] A. Veligura, H. J. van Elferen, N. Tombros, J. C. Maan, U. Zeitler, and B. J. van Wees, Transport gap in suspended bilayer graphene at zero magnetic field, Phys. Rev. B **85**, 155412 (2012).
[62] A. N. Kolmogorov and V. H. Crespi, Registry-dependent interlayer potential for graphitic systems, Phys. Rev. B **71**, 235415 (2005).
[63] I. V. Lebedeva, A. A. Knizhnik, A. M. Popov, Y. E. Lozovik, and B. V. Potapkin, Interlayer interaction and relative vibrations of bilayer graphene, Phys. Chem. Chem. Phys. **13**, 5687 (2011).
[64] R. R. Del Grande, M. G. Menezes, and R. B. Capaz, Layer breathing and shear modes in multilayer graphene: a DFT-vdW study, J. Phys.: Condens. Matter **31**, 295301 (2019).
[65] A. S. Mayorov, D. C. Elias, M. Mucha-Kruczynski, R. V. Gorbachev, T. Tudorovskiy, A. Zhukov, S. V. Morozov, M. I. Katsnelson, V. I. Fal'ko, A. K. Geim *et al.*, Interaction-driven spectrum reconstruction in bilayer graphene, Science **333**, 860 (2011).
[66] Y. Nam, D.-K. Ki, D. Soler-Delgado, and A. F. Morpurgo, A family of finite-temperature electronic phase transitions in graphene multilayers, Science **362**, 324 (2018).
[67] Y. Liu, W. S. Lew, and Z. Liu, Observation of anomalous resistance behavior in bilayer graphene, Nanoscale Res. Lett. **12**, 1 (2017).
[68] B. Butz, C. Dolle, F. Niekiel, K. Weber, D. Waldmann, H. B. Weber, B. Meyer, and E. Spiecker, Dislocations in bilayer graphene, Nature (London) **505**, 533 (2014).
[69] V. M. Pereira, R. M. Ribeiro, N. M. R. Peres, and A. H. Castro Neto, Distortion of the perfect lattice structure in bilayer graphene, Phys. Rev. B **79**, 045421 (2009).
[70] H. P. Dahal, T. O. Wehling, K. S. Bedell, J.-X. Zhu, and A. V. Balatsky, Charge inhomogeneity in a single and bilayer graphene, Phys. B: Condens. Matter **405**, 2241 (2010).
[71] J. Nilsson, A. H. C. Neto, N. M. R. Peres, and F. Guinea, Electron-electron interactions and the phase diagram of a graphene bilayer, Phys. Rev. B **73**, 214418 (2006).
[72] A. Flachi, Strongly interacting fermions and phases of the Casimir effect, Phys. Rev. Lett. **110**, 060401 (2013).